Helicity transitions and emerging superconductivity in chiral α-HgS

He Zhang [1,2] Wei Zhong [3] Yanghao Meng,[1,2] Bowen Tang,[1] Binbin Yue [3,*] Xiaohui Yu,[1,2,4,†] and Fang Hong [1,2,4,‡]

[1]*Beijing National Laboratory for Condensed Matter Physics, Institute of Physics, Chinese Academy of Sciences, Beijing 100190, China*
[2]*School of Physical Sciences, University of Chinese Academy of Sciences, Beijing 100049, China*
[3]*Center for High Pressure Science and Technology Advanced Research, 10 East Xibeiwang Road, Haidian, Beijing 100094, China*
[4]*Songshan Lake Materials Laboratory, Dongguan, Guangdong 523808, China*

A helical structure shows a naturally fluctuating behavior in charge distribution, analogous, to some extent, to the charge density wave. It is an open question whether superconductivity can be induced by suppressing the helical structure in a largely gapped system. Here, we report the superconductivity in chiral α-HgS with a band gap of 1.9 eV after a pressure-driven helical-nonhelical transition. The maximum critical temperature (T_c) reaches 11 K at 25.4 GPa, and the T_c-critical magnetic field (B_{c2}) relation exhibits multiband features. Furthermore, an isostructural-like transition, together with a transition of direct-indirect band gaps, is presented due to the reduced distance of the helical chains near 8 GPa, at which the second harmonic generation shows a strong response. Phonon softening plays a key role in the stability of the helical structure and the emergence of superconductivity. This Letter may inspire the exploration of superconductivity and other new physics in other helical/chiral systems and will extend our understanding of the versatile behavior in such kinds of materials.

Chirality refers to the inherent asymmetry preventing an object from superimposing onto its mirror image, breaking spatial inversion and reflection symmetries, which is one of the basic nature properties that is significant in many fields from condensed matter physics to analytical chemistry, molecular biology, and crystallography [1,2]. The chirality generally produces intriguing physical phenomena, such as optical dichroism, chirality-induced spin selectivity, and asymmetric scattering of polarized electrons [3,4]. In chiral superconductors, the noncentrosymmetric structure may favor a triplet *p*-wave superconductivity [5]. Meanwhile, magnetism can also show spin chirality, showing large magneto-optical dichroism [6] and new magnetic states, such as magnetic skyrmions [7]. Helical structures are special types of chiral structures with a screw axis, and DNA is a representative example. In inorganic materials, the helical structures can bring about some unconventional phenomena. For example, the metallic helical crystals trigonal $TaRh_2B_2$, $NbRh_2B_2$ [8–10], and hexagonal $(Pt_{0.2}Ir_{0.8})_3Zr_5$ [11] display superconductivity with anomalous upper critical field values that exceed the Pauli limit. Helical tungsten disulfide nanotubes display nonreciprocity behavior with nonequivalent forward and backward supercurrent flows [12]. Recently, the chirality-induced selectivity of phonon angular momenta has been observed in helical quartz [13,14]. These works significantly advance our understanding of how chiral and/or helical structures impact the materials' properties, and inspire us to study or manipulate the properties in helical systems by artificial methods.

α-HgS is a typical chiral material with threefold helical chains, standing out from other monosulfides with predominantly cubic or hexagonal structures, as outlined in Table S1 in the Supplemental Material [15] (see also Refs. [16–36] therein). Recently, chiral phonon splitting in α-HgS has been observed by circularly polarized Raman spectroscopy [37]. The cinnabar phase's space group is a subgroup of the NaCl phase, so the cinnabar structure could be regarded as a distorted cubic structure. The helical structure shows a naturally periodic fluctuation of charge distribution, and it gives a few satellite diffraction peaks near the main peaks of the NaCl structure (Fig. 1), which is analogous to the satellite diffractions from the charge density wave (CDW) in many materials. It has been reasoned that there is a high chance to observe superconductivity near a critical point where CDW is suppressed [38]. Motivated by this idea, will HgS turn into a superconductor when its CDW-like helical structure is suppressed? A positive answer is given by this Letter.

Here, we report the superconductivity in HgS by suppressing the helical chain structure via pressure. Meanwhile, the x-ray diffraction (XRD) reveals an isostructural-like transition with a change in the c/a ratio near 8 GPa, at which α-HgS undergoes an electronic phase transition from a direct band gap to an indirect band gap, and second harmonic generation (SHG) shows a strong response. Importantly, T_c reaches 11 K at 25.4 GPa, which is also the highest one among NaCl-type metal sulfide superconductors. Clear phonon softening behavior is observed and is responsible for the structural instability of the helical phase and consequent superconductivity. This Letter provides a different strategy or paradigm to search for superconductivity in CDW-like helical systems and may extend our knowledge of chiral materials.

Multiple experiments were conducted to investigate various aspects of HgS under pressure, including the crystal

*Contact author: yuebb@hpstar.ac.cn
†Contact author: yuxh@iphy.ac.cn
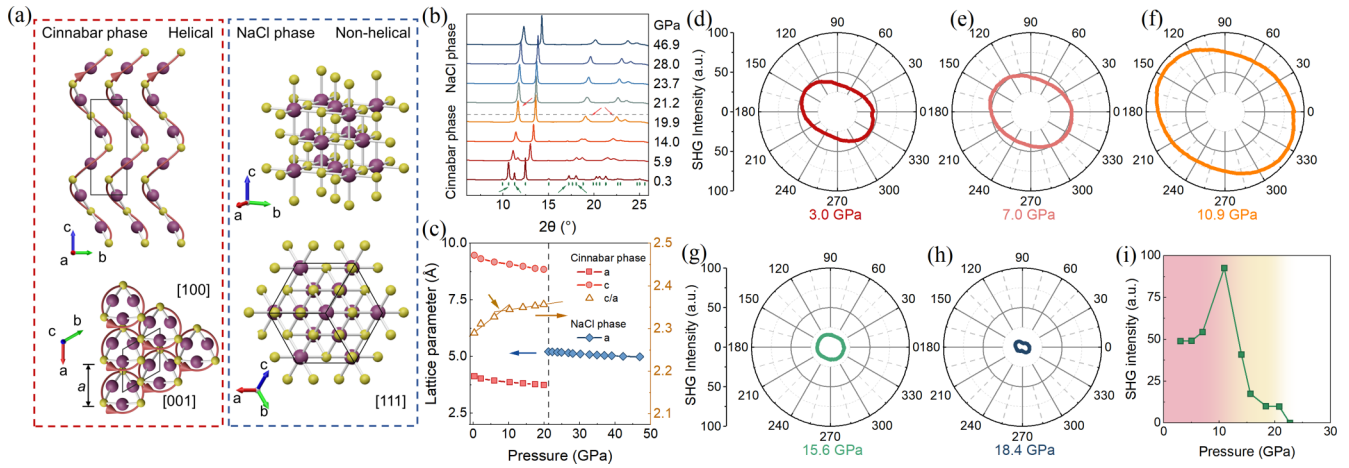‡Contact author: hongfang@iphy.ac.cn

FIG. 1. Atomic structures, phase transitions, and second harmonic generation in HgS under pressure. (a) The atomic structures of cinnabar phase $P3_121$ (space group No. 152) at ambient pressure and NaCl phase $Fm\bar{3}m$ (space group No. 225) at high pressure. Yellow and purple balls represent S atoms and Hg atoms. The helical chains are displayed along different directions. (b) The XRD patterns of HgS with an x-ray wavelength of 0.6199 Å under pressure up to 46.9 GPa. Green short lines mark the Bragg positions at ambient pressure. (c) The lattice parameters of the cinnabar phase and NaCl phase under pressure. (d)–(h) Polarization-resolved SHG measurements of HgS at various pressures. (i) The pressure dependence of maximum SHG intensity. A peak is somewhat consistent with the kink point of the lattice parameter c/a ratio as presented in (c).

structure, helicity transition, electronic structure, phonon behaviors, electric transport properties, and ac susceptibility measurements. Synchrotron x-ray diffraction (XRD) and SHG were employed to track the evolution of the helical structure of HgS. Raman spectroscopy and ultraviolet-to-visible-to-near-infrared (UV-vis-NIR) absorption spectroscopy were utilized to investigate its vibrational modes and electronic structure. Optical experiments were conducted using symmetric diamond anvil cells (DACs), electrical transport properties were examined using a BeCu DAC with the standard four-probe method, and ac susceptibility was measured by the mutual induction method. Further details on the experimental methods can be found in the Supplemental Material [15].

The helical α-HgS crystallizes in the cinnabar phase (space group No. $P3_121$). Upon compression, the helical structure will be suppressed and transformed to a nonhelical NaCl structure (space group No. $Fm\bar{3}m$) at 21 GPa. The helical chain structure of HgS shows a spacing of a between the two closest chains and a repeating unit length of c, as shown in Fig. 1(a). Under compression, the chains are close enough to connect with each other and construct a cubic lattice [39]. The phase transition process is examined by x-ray diffraction (XRD) and SHG as shown in Fig. 1 (see Fig. S1 in the Supplemental Material [15] for complete XRD patterns and the structure sequence). The structural phase transition from the cinnabar phase to the NaCl phase happens at around 21 GPa. In the patterns of the cinnabar phase, there are some weak diffraction peaks near the NaCl main peaks, which show a similarity to the satellite peaks in CDW systems, as shown in Fig. 1(b).

More structural details of HgS under pressure are obtained by refinement, such as lattice parameters, unit cell volumes, and Hg-S bond lengths of HgS under pressure [see Fig. 1(c) and Fig. S2 in the Supplemental Material [15]]. The lattice parameter a is more compressible than c, with c/a increasing with pressure. A kink is presented near 8 GPa in the pressure-dependent c/a, as indicated by the dark yellow arrow in Fig. 1(c), suggesting an isostructural-like transition. The lattice parameters and atomic positions of the two phases are listed in Table S2 in the Supplemental Material [15]. The evolution gives the picture that the pressure effect on the approaching interchain is greater than the in-chain contraction.

The SHG experiments on single-crystal HgS were conducted to provide detailed information about the helicity transition. The polar plots depicting polarization-resolved SHG [Figs. 1(d)–1(h)] showcase apparent SHG signals, revealing the noncentrosymmetric nature of helical HgS. Throughout the compression process, the anisotropy of the polarization curve remains almost unchanged, indicating the absence of any symmetric or structural transition below 21 GPa. The maximum intensity is shown in Fig. 1(i), and it is clear that between 7 and 10.9 GPa, the SHG intensity shows a maximum. The intensity then decreases with further compression. At around 21 GPa, a sudden disappearance of the SHG signal marks the noncentrosymmetric (helical) to centrosymmetric (nonhelical) structural transition. This observation aligns with the pressure response of HgS as indicated by our x-ray diffraction results. The kink behavior of the pressure-dependent SHG intensity between 7 and 10.9 GPa is also well consistent with the isostructural-like transition around 8 GPa as mentioned above.

The Raman spectra of HgS under pressure further confirm the phase transition at 21 GPa and show a prominent phonon softening behavior in the cinnabar phase. The cinnabar phase has a point group of D_3 and vibrational modes of $2A_1 + 3A_2 + 5E$. Two A_1 modes are Raman active, three A_2 modes are inferred active, and five E modes are active in both Raman and inferred spectroscopy. The main peaks at 253.6 and 45.1 cm^{-1} are A_1 modes [40], called the chain breathing modes: atomic displacements in the ab plane along the direction per-
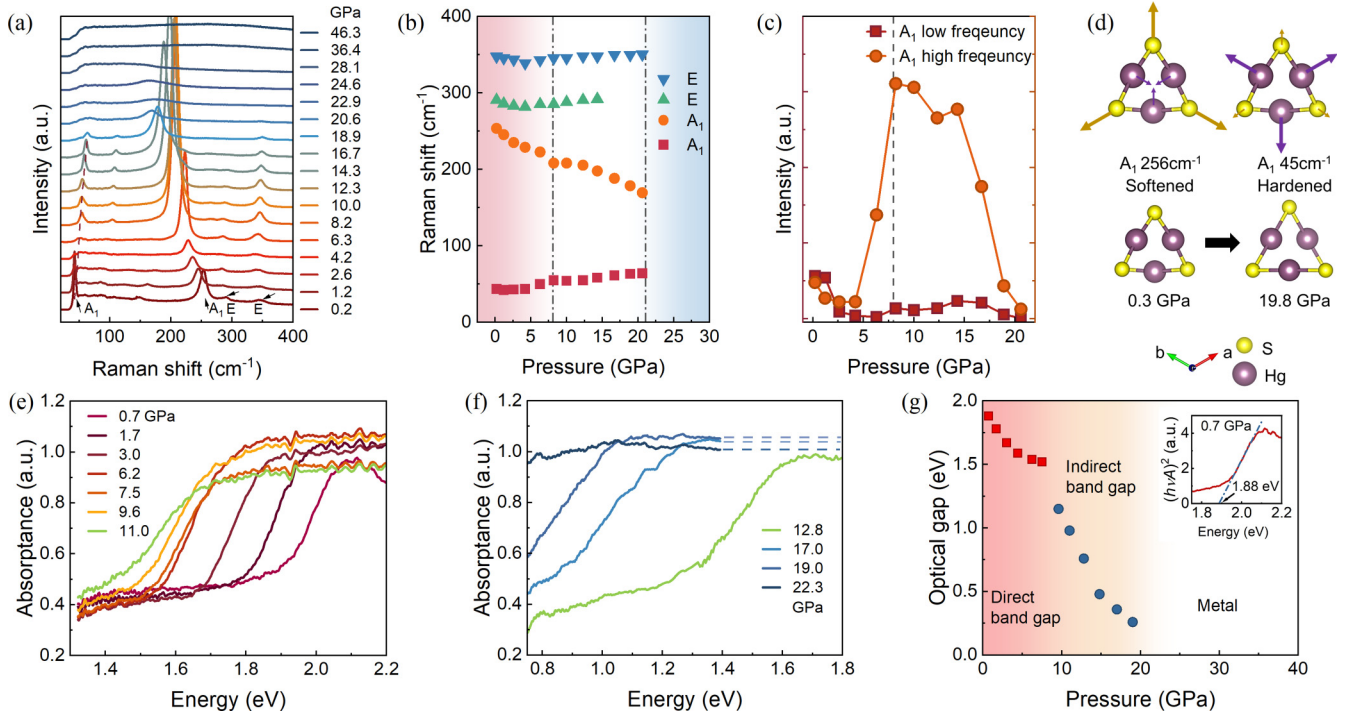
FIG. 2. The phonon softening and electronic transitions of HgS under pressure investigated by Raman and UV-VIS-NIR absorption spectroscopy. (a) The sequence of Raman spectra of HgS under compression. (b) The position of Raman peaks is modulated by pressure. Dashed lines separate different phase regions. (c) The intensity evolution of two A_1 modes. (d) The schematic diagrams of atomic motions of A_1 modes and the chain-structure evolution projected onto the ab plane. (e), (f) UV-VIS-NIR absorption spectra. (g) The optical band-gap evolution obtained by the Tauc plot method. The inset shows the linear extrapolation and the optical band gap is the intercept.

pendicular to the c axis, corresponding to two different bases, nearly pure S motions with a higher frequency and pure Hg motions with a lower frequency [41]. Upon compression, two A_1 modes show a competition relation under pressure: The high-frequency A_1 mode becomes softened while the low-frequency A_1 mode becomes hardened, as seen in Figs. 2(a) and 2(b). Most Raman peaks are widened and indistinguishable above 21 GPa, corresponding to the metallization and structural transition. In addition, both A_1 modes exhibit an abnormal enhancement in intensity above 6.3 GPa and reach a maximum intensity at 8.2 GPa [Fig. 2(c)], consistent with the isostructural phase transition. The intensity anomaly was also observed during decompression (see Fig. S3 in the Supplemental Material [15]). The atomic displacements of two A_1 modes are presented in Fig. 2(d): With increasing pressure, the Hg atoms are closer while the in-chain Hg-S bond experiences a slight stretching, causing the low-frequency A_1 mode with Hg motions to be hardened, while the high-frequency A_1 mode with S motions is softened. Consequently, the distorted HgS triangle prefers to be in a nondistorted triangle under high pressure.

The phonon anomaly and softening are generally accompanied with a transition of electronic behavior. To check for a possible electronic transition, optical absorption spectra under pressure are collected as shown in Figs. 2(e) and 2(f). HgS is a semiconductor/insulator with a direct band gap of 1.9 eV at 0.7 GPa. A clear absorption edge can be observed in the low-pressure range, which moves to lower energy with increasing pressure, indicating a reduced band gap. The Tauc plot method

[42] is used to obtain the optical band gap, and more details are shown in Fig. S4 in the Supplemental Material [15]. Below 9.6 GPa, the absorption edges show a redshift with increasing pressure and approach to a constant. After 9.6 GPa, the absorption gap changes dramatically with pressure, and the absorption edge is slightly widened, so an indirect band gap is preferred in this case. By analyzing the intercept of the linear fitting line, the direct optical band gaps, indirect band gaps, and their pressure dependence are obtained as shown in Fig. 2(g). Prior first-principles calculations have claimed that the cinnabar phase is a direct band-gap semiconductor at pressures below 8 GPa and an indirect band-gap semiconductor above 8 GPa [43]. This matches well with our results. Hence, the isostructural phase transition results in an electronic phase transition and abnormal phonon intensity change, suggesting a strong electron-phonon coupling.

A superconductivity transition is directly observed at 22.9 GPa by electrical transport measurements, as displayed in Fig. 3, and phonon softening and structure instability are responsible for that. Below 15.9 GPa, the resistance of HgS is too large and out of the detection limit in our experimental setup. The sample still behaves as a semiconductor at 15.9 GPa and the resistance increases significantly from 10^3 Ω at 300 K to 10^7 Ω below 2 K, as seen in Fig. 3(a). The resistance decreases overall monotonously with pressure, indicating a continuously reduced band gap under pressure. At 22.9 GPa, the sample turns into a metal and shows superconductivity with a T_c of 5.4 K (T_c without special instructions stands for $T_c^{90\%}$ where the resistance drops to 90% of the
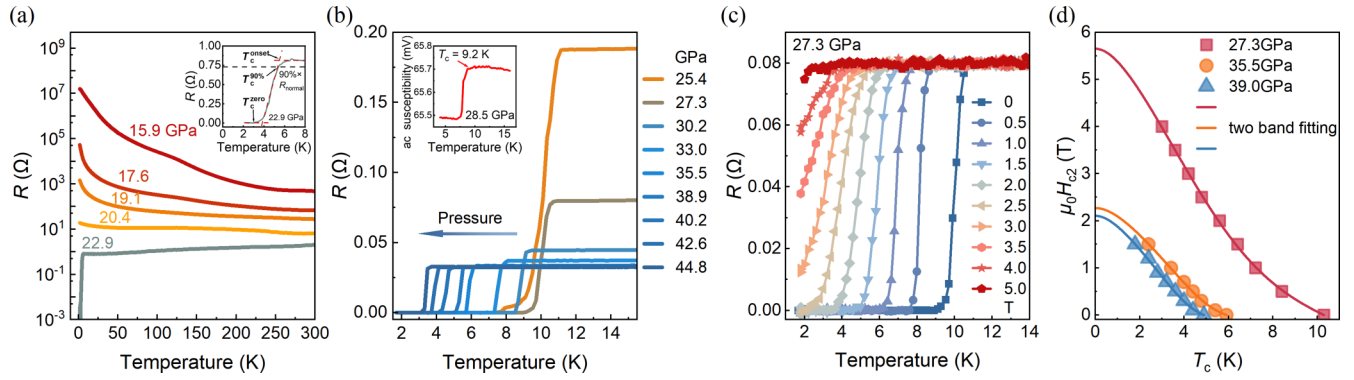
FIG. 3. The insulator-metal transition and superconductivity of HgS under pressure. (a) The R-T curves are from 15.9 to 22.9 GPa. The inset shows the criteria of T_c^{onset}, $T_c^{90\%}$, and T_c^{zero}. (b) The R-T curves are from 25.4 to 44.8 GPa. The inset shows the ac susceptibility signal at 28.5 GPa which is consistent with the resistance measurement. (c) Superconductivity transition under different external magnetic fields at 27.3 GPa. (d) Two band fittings of upper critical magnetic fields and T_c relations at three different pressures.

normal state value), as shown in the inset of Fig. 3(a). The SC transition becomes shaper, T_c is enhanced, and reaches 11.0 K at 25.4 GPa, above which the superconductivity is gradually suppressed though the metallic behavior of the sample becomes better, as seen in Fig. 3(b).

To confirm the superconductivity of HgS under pressure, an ac magnetic susceptibility measurement was also conducted. The diamagnetic signal is evident in the inset of Fig. 3(b), with a T_c of 9.2 K at 28.5 GPa, consistent with the resistance measurements. Thus, both resistance and ac susceptibility measurements conclusively demonstrate the superconductivity of HgS under compression.

Conventional BCS theory [44] and the McMillan strong-coupling theory [45] state that superconductivity arises from phonon-mediated electron pairing. The superconducting properties depend on the electron-phonon coupling λ, which is inversely proportional to the average squared phonon frequency. So the phonon softening lowering the frequency distribution could enhance the electron-phonon coupling and promote superconductivity [46]. This phenomenon is observed across many conventional and high-temperature superconductors, such as doping-dependent phonon softening in YBa$_2$Cu$_3$O$_7$ and HgBa$_2$CuO$_4$ [47,48] as well as element superconductors Sn and Pb [49,50]. For HgS, the softened in-chain A_1 mode during the structural evolution contributes to the structural transition and superconductivity. As can be seen in Fig. 3(a), the superconductivity emerges along with the metallization, without a non-SC metal intermediate state.

We investigate the magnetic field effect on the superconductivity of HgS up to 5.0 T. At 27.3 GPa, the zero-field T_c is 10.3 K, and it decreases with increasing field, as seen in Fig. 3(c). When the magnetic field reaches 5 T, the SC is barely identified at 1.7 K. Meanwhile, the SC transition becomes broader with increasing external magnetic field. Both phenomena confirm the superconductivity of HgS. Magnetic field versus T_c under three different pressures is shown in Fig. 3(d). The curvature behavior in the low magnetic field range is noteworthy, and the Ginzburg-Landau (GL) fitting is not applicable. Since NaCl-type HgS has a high-symmetry structure, the anisotropic single-band superconductivity is excluded, and the curvature at low fields is attributed to multi-

band superconductivity. The zero-temperature upper critical magnetic field at 27.3 GPa is around 5.65 T by two-band fitting. That is much higher than the 1.2 T at 100 GPa for pure sulfur [51,52]. A previous calculation shows that the d electrons of Hg and the p electrons of S mainly contribute to the density of states (DOS) [43] in the NaCl phase HgS. It is noted that the T_c in pure Hg decreases with pressure [53] (apart from 4.2 K with pressure), while the T_c of sulfur is enhanced with pressure from 10 to 17 K [51,52]. In this case, p electrons in S may still dominate the contribution to the superconductivity but are modulated by the crystal field stabilized by Hg. Due to the much larger mass of Hg, the overall phonon frequency will decrease compared to pure S, which results in a declining trend of T_c with pressure in HgS. HgS has the highest upper critical field and high T_c close to 11.0 K compared to other metal monosulfides [54–60] (Fig. S5 in the Supplemental Material [15]).

The comprehensive experiments reveal a clear structural transition in HgS from a helical cinnabar phase to a nonhelical NaCl phase at 21 GPa, and emerging superconductivity. Based on these results, a phase diagram of HgS under pressure is proposed in Fig. 4. The evolution of the band gap and T_c under pressure is clearly shown, while a linear relationship between lattice parameter and T_c is demonstrated in Fig. S6 in the Supplemental Material [15]. Besides HgS, similar behavior was also observed in helical Se and Te with narrower gaps of 0.88 and 0.19 eV [51,52,61]. The semiconductor-metal transition of Te happens at 4 GPa, with the structural transition from the helical chain structure to the superconducting monoclinic Te-II phase [62,63]. The semiconducting Se-I phase undergoes a metal transition to the Se-II phase when the helical structure vanishes, and superconductivity develops in the Se-III phase at 23 GPa, which is isostructural with Te-II [63,64]. It is noted that either Te or Se transform from a high-symmetry trigonal $P3_121$ (space group No. 152) structure to a low-symmetry monoclinic phase or even a triclinic $P\bar{1}$ (space group No. 2) phase [65]. This structural phase transition differs from that in a CDW and superconductivity competing system, where the system is expected to transform from a low-symmetry phase to a high-symmetry phase as superconductivity emerges [38,66]. Therefore, it is difficult to judge the role of helicity
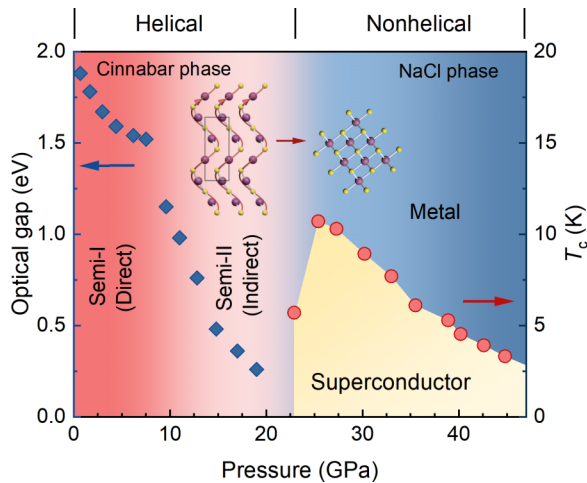
FIG. 4. Phase diagram displays the band gap and T_c evolution of HgS under pressure, and the superconducting region is clearly shown in yellow.

on superconductivity in these gapped helical systems. In this case, α-HgS has been an ideal platform to understand the relation between structural helicity and superconductivity.

It has been more than 100 years since superconductivity was first discovered, while it has been always a mystery to obtain specific rules to search for potential superconductors. There seems to be a higher chance to observe superconductivity in a system with multiple competing orderings, such as the charge density wave (CDW) [38], spin density wave (SDW) [67,68], and the recently confirmed pair density wave (PDW) [69], as superconductivity could emerge after suppressing these orderings. The common feature among these orderings is their long-range modulation, which opens a gap on a scale of a few meV to tens of meV. Here, the lattice

distortion/density-wave-like state (LDW) in largely gapped systems such as HgS plays a role as an alternative wave form and it is promising to be strongly correlated with the superconductivity. This long-range distortion modulation not only extends the scope of CDW, but also provides a different paradigm to search for new superconductors.

In summary, we propose another way to realize superconductivity in a special type of chiral material with a helical chain structure. The natural fluctuation of charge distribution in helical materials resembles the charge density wave. The atomic distortion in helical HgS opens a large band gap rather than a much smaller gap in most CDW materials, however, such a distortion and large band gap can be well controlled by external pressure. When the helical phase is fully suppressed by pressure, the band gap is closed and superconductivity emerges in HgS. The Raman anomaly and electronic phase transition suggest a strong electron-phonon coupling effect. The phonon softening is very significant and it is responsible for the structural instability of the helical phase and consequent superconductivity. Our study on HgS will stimulate the exploration of superconductivity or other exotic physics in other similar helical materials.

[1] R. S. Cahn, C. Ingold, and V. Prelog, Specification of molecular chirality, Angew. Chem. Int. Ed. Engl. **5**, 385 (1966).

[2] J. Gal, Pasteur and the art of chirality, Nat. Chem. **9**, 604 (2017).

[3] F. Evers, A. Aharony, N. Bar-Gill, O. Entin-Wohlman, P. Hedegård, O. Hod, P. Jelinek, G. Kamieniarz, M. Lemeshko, K. Michaeli, V. Mujica, R. Naaman, Y. Paltiel, S. Refaely-Abramson, O. Tal, J. Thijssen, M. Thoss, J. M. van Ruitenbeek, L. Venkataraman, D. H. Waldeck *et al.*, Theory of chirality induced spin selectivity: Progress and challenges, Adv. Mater. **34**, 2106629 (2022).

[4] K. Ray, S. P. Ananthavel, D. H. Waldeck, and R. Naaman, Asymmetric scattering of polarized electrons by organized organic films of chiral molecules, Science **283**, 814 (1999).

[5] C. Kallin and J. Berlinsky, Chiral superconductors, Rep. Prog. Phys. **79**, 054502 (2016).

[6] M. Saito, K. Ishikawa, K. Taniguchi, and T. Arima, Magnetic control of crystal chirality and the existence of a large magneto-optical dichroism effect in CuB$_2$O$_4$, Phys. Rev. Lett. **101**, 117402 (2008).

[7] S.-H. Yang, R. Naaman, Y. Paltiel, and S. S. P. Parkin, Chiral spintronics, Nat. Rev. Phys. **3**, 328 (2021).

[8] E. M. Carnicom, W. Xie, T. Klimczuk, J. Lin, K. Górnicka, Z. Sobczak, N. P. Ong, and R. J. Cava, TaRh$_2$B$_2$ and NbRh$_2$B$_2$: Superconductors with a chiral noncentrosymmetric crystal structure, Sci. Adv. **4**, eaar7969 (2018).

[9] D. A. Mayoh, A. D. Hillier, K. Götze, D. M. Paul, G. Balakrishnan, and M. R. Lees, Multigap superconductivity in chiral noncentrosymmetric TaRh$_2$B$_2$, Phys. Rev. B **98**, 014502 (2018).

[10] J. Islam, M. A. Rahman, and A. K. M. A. Hossain, Physical and superconducting properties of chiral noncentrosymmetric TaRh$_2$B$_2$ and NbRh$_2$B$_2$: A comprehensive DFT study, ACS Appl. Electron. Mater. **4**, 1143 (2022).

[11] Y. Watanabe, H. Arima, A. Yamashita, A. Miura, C. Moriyoshi, Y. Goto, C.-H. Lee, R. Higashinaka, H. Usui, S. Kawaguchi, K. Hoshi, and Y. Mizuguchi, Low-temperature chiral crystal structure and superconductivity in (Pt$_{0.2}$Ir$_{0.8}$)$_3$Zr$_5$, J. Am. Chem. Soc. **146**, 773 (2024).

[12] F. Qin, W. Shi, T. Ideue, M. Yoshida, A. Zak, R. Tenne, T. Kikitsu, D. Inoue, D. Hashizume, and Y. Iwasa, Superconductivity in a chiral nanotube, Nat. Commun. **8**, 14465 (2017).

[13] K. Ohe, H. Shishido, M. Kato, S. Utsumi, H. Matsuura, and Y. Togawa, Chirality-induced selectivity of phonon angular momenta in chiral quartz crystals, Phys. Rev. Lett. **132**, 056302 (2024).

[14] H. Ueda, M. García-Fernández, S. Agrestini, C. P. Romao, J. van den Brink, N. A. Spaldin, K.-J. Zhou, and U. Staub, Chiral phonons in quartz probed by X-rays, Nature (London) **618**, 946 (2023).

[15] See Supplemental Material at http://link.aps.org/supplemental/10.1103/PhysRevB.110.L060502 for experimental methods, outline of metal monosulfides, Raman spectroscopy, electric transport measurements during decompression, the Tauc plot method, critical temperature, ac magnetic susceptibility measurement, and the lattice parameter relationship, which includes Refs. [16–36,54,56–59].

[16] A. Maachou, H. Aboura, B. Amrani, R. Khenata, S. Bin Omran, and D. Varshney, Structural stabilities, elastic and thermodynamic properties of scandium chalcogenides via first-principles calculations, Comput. Mater. Sci. **50**, 3123 (2011).

[17] L. T. Nguyen and G. Makov, GeS phases from first-principles: Structure prediction, optical properties, and phase transitions upon compression, Cryst. Growth Des. **22**, 4956 (2022).

[18] K. Knorr, L. Ehm, M. Hytha, B. Winkler, and W. Depmeier, The high-pressure α/β phase transition in lead sulphide (PbS), Eur. Phys. J. B **31**, 297 (2003).

[19] X. Ji, Y. Yu, J. Ji, J. Long, J. Chen, and D. Liu, Theoretical studies of the pressure-induced phase transition and elastic properties of BeS, J. Alloys Compd. **623**, 304 (2015).

[20] S. M. Peiris, J. S. Sweeney, A. J. Campbell, and D. L. Heinz, Pressure-induced amorphization of covellite, CuS, J. Chem. Phys. **104**, 11 (1996).

[21] H. K. Mao, J. Xu, and P. M. Bell, Calibration of the ruby pressure gauge to 800 kbar under quasi-hydrostatic conditions, J. Geophys. Res.: Solid Earth **91**, 4673 (1986).

[22] A. Moodenbaugh, D. Johnston, R. Viswanathan, R. Shelton, L. DeLong, and W. Fertig, Superconductivity of transition metal sulfides, selenides, and phosphides with the NaCl structure, J. Low Temp. Phys. **33**, 175 (1978).

[23] X. Yang, Y. Wang, K. Wang, Y. Sui, M. Zhang, B. Li, Y. Ma, B. Liu, G. Zou, and B. Zou, Polymorphism and formation mechanism of nanobipods in manganese sulfide nanocrystals induced by temperature or pressure, J. Phys. Chem. C **116**, 3292 (2012).

[24] A. J. Campbell and D. L. Heinz, Equation of state and high pressure phase transition of NiS in the NiAs structure, J. Phys. Chem. Solids **54**, 5 (1993).

[25] P. Jha, U. K. Sakalle, and S. P. Sanyal, Pressure induced structural phase transition in MgS and CaS, J. Phys. Chem. Solids **59**, 599 (1998).

[26] A. Rabkin, S. Samuha, R. E. Abutbul, V. Ezersky, L. Meshi, and Y. Golan, New nanocrystalline materials: a previously unknown simple cubic phase in the SnS binary system, Nano Lett. **15**, 2174 (2015).

[27] R. Khenata, H. Baltache, M. Rérat, M. Driz, M. Sahnoun, B. Bouhafs, and B. Abbar, First-principle study of structural, electronic and elastic properties of SrS, SrSe and SrTe under pressure, Phys. B: Condens. Matter **339**, 208 (2003).

[28] F. M. Hashimzade, D. A. Huseinova, Z. A. Jahangirli, and B. H. Mehdiyev, Second-order phase transition at high-pressure in GeS crystal, Phys. B: Condens. Matter **454**, 56 (2014).

[29] Y. Gupta, M. M. Sinha, and S. S. Verma, On the potential for superconductivity in ZrX (X = S and Te): a first-principles study, Physica C **577**, 1353714 (2020).

[30] H. M. Tütüncü and G. P. Srivastava, *Ab initio* investigations of phonon anomalies and superconductivity in the rock-salt YS, Philos. Mag. **87**, 4109 (2007).

[31] S. T. Weir, Y. K. Vohra, and A. L. Ruoff, High-pressure phase transitions and the equations of state of BaS and BaO, Phys. Rev. B **33**, 4221 (1986).

[32] H. Luo, R. G. Greene, K. Ghandehari, T. Li, and A. L. Ruoff, Structural phase transformations and the equations of state of calcium chalcogenides at high pressure, Phys. Rev. B **50**, 16232 (1994).

[33] S. Desgreniers, L. Beaulieu, and I. Lepage, Pressure-induced structural changes in ZnS, Phys. Rev. B **61**, 8726 (2000).

[34] M. Durandurdu, *Cmcm* phase of GeS at high pressure, Phys. Rev. B **72**, 144106 (2005).

[35] N. Benkhettou, D. Rached, B. Soudini, and M. Driz, High-pressure stability and structural properties of CdS and CdSe, Phys. Status Solidi B **241**, 101 (2004).

[36] J. Gao, J. Liu, Q. Zhang, G. Qi, and W. Jiao, Theoretical investigation of the phase transition, elastic and superconductivity properties of LaS under pressure, J. Supercond. Novel Magn. **27**, 2455 (2014).

[37] K. Ishito, H. Mao, Y. Kousaka, Y. Togawa, S. Iwasaki, T. Zhang, S. Murakami, J.-I. Kishine, and T. Satoh, Truly chiral phonons in α-HgS, Nat. Phys. **19**, 35 (2023).

[38] A. M. Gabovich, A. I. Voitenko, and M. Ausloos, Charge- and spin-density waves in existing superconductors: competition between cooper pairing and Peierls or excitonic instabilities, Phys. Rep. **367**, 583 (2002).

[39] T. Huang and A. L. Ruoff, Pressure-induced phase transition of HgS, J. Appl. Phys. **54**, 5459 (1983).

[40] S. V. Gotoshia and L. V. Gotoshia, Laser Raman and resonance Raman spectroscopies of natural semiconductor mineral cinnabar, α-HgS, from various mines, J. Phys. D: Appl. Phys. **41**, 115406 (2008).

[41] R. Zallen, G. Lucovsky, W. Taylor, A. Pinczuk, and E. Burstein, Lattice vibrations in trigonal HgS, Phys. Rev. B **1**, 4058 (1970).

[42] J. Tauc, R. Grigorovici, and A. Vancu, Optical properties and electronic structure of amorphous germanium, Phys. Status Solidi B **15**, 627 (1966).

[43] S.-R. Sun, Y.-C. Li, J. Liu, Y.-H. Dong, and C.-X. Gao, Electronic structures and metallization of HgS under high pressures: First principles calculations and resistivity measurements, Phys. Rev. B **73**, 113201 (2006).

[44] J. Bardeen, L. N. Cooper, and J. R. Schrieffer, Theory of superconductivity, Phys. Rev. **108**, 1175 (1957).

[45] W. L. McMillan, Transition temperature of strong-coupled superconductors, Phys. Rev. **167**, 331 (1968).

[46] P. B. Allen and M. L. Cohen, Superconductivity and phonon softening, Phys. Rev. Lett. **29**, 1593 (1972).

[47] H. Uchiyama, A. Q. R. Baron, S. Tsutsui, Y. Tanaka, W. Z. Hu, A. Yamamoto, S. Tajima, and Y. Endoh, Softening of Cu-O bond stretching phonons in tetragonal HgBa$_2$CuO$_{4+\delta}$, Phys. Rev. Lett. **92**, 197005 (2004).

[48] L. Pintschovius, D. Reznik, W. Reichardt, Y. Endoh, H. Hiraka, J. M. Tranquada, H. Uchiyama, T. Masui, and S. Tajima, Oxy-

gen phonon branches in YBa$_2$Cu$_3$O$_7$, Phys. Rev. B **69**, 214506 (2004).

[49] K. Houben, J. K. Jochum, S. Couet, E. Menéndez, T. Picot, M. Y. Hu, J. Y. Zhao, E. E. Alp, A. Vantomme, K. Temst, and M. J. Van Bael, The influence of phonon softening on the superconducting critical temperature of Sn nanostructures, Sci. Rep. **10**, 5729 (2020).

[50] S. Bose, C. Galande, S. P. Chockalingam, R. Banerjee, P. Raychaudhuri, and P. Ayyub, Competing effects of surface phonon softening and quantum size effects on the superconducting properties of nanostructured Pb, J. Phys.: Condens. Matter **21**, 205702 (2009).

[51] S. Kometani, M. I. Eremets, K. Shimizu, M. Kobayashi, and K. Amaya, Observation of pressure-induced superconductivity of sulfur, J. Phys. Soc. Jpn. **66**, 2564 (1997).

[52] V. V. Struzhkin, R. J. Hemley, H.-k. Mao, and Y. A. Timofeev, Superconductivity at 10–17 K in compressed sulphur, Nature (London) **390**, 382 (1997).

[53] L. D. Jennings and C. A. Swenson, Effects of pressure on the superconducting transition temperatures of Sn, In, Ta, Tl, and Hg, Phys. Rev. **112**, 31 (1958).

[54] Arushi, R. K. Kushwaha, D. Singh, A. D. Hillier, M. S. Scheurer, and R. P. Singh, Time-reversal symmetry breaking in the superconducting state of ScS, Phys. Rev. B **106**, L020504 (2022).

[55] R. Matsumoto, P. Song, S. Adachi, Y. Saito, H. Hara, A. Yamashita, K. Nakamura, S. Yamamoto, H. Tanaka, T. Irifune, H. Takeya, and Y. Takano, Pressure-induced superconductivity in tin sulfide, Phys. Rev. B **99**, 184502 (2019).

[56] H. Zhang, W. Zhong, Y. Meng, B. Yue, X. Yu, J.-T. Wang, and F. Hong, Superconductivity above 12 K with possible multiband features in CsCl-type PbS, Phys. Rev. B **107**, 174502 (2023).

[57] L.-C. Chen, H. Yu, H.-J. Pang, B.-B. Jiang, L. Su, X. Shi, L.-D. Chen, and X.-J. Chen, Pressure-induced superconductivity in palladium sulfide, J. Phys.: Condens. Matter **30**, 155703 (2018).

[58] J. Zhang, F.-L. Liu, T.-P. Ying, N.-N. Li, Y. Xu, L.-P. He, X.-C. Hong, Y.-J. Yu, M.-X. Wang, J. Shen, W.-G. Yang, and S.-Y. Li, Observation of two superconducting domes under pressure in tetragonal FeS, npj Quantum Mater. **2**, 49 (2017).

[59] X. Lai, H. Zhang, Y. Wang, X. Wang, X. Zhang, J. Lin, and F. Huang, Observation of superconductivity in tetragonal FeS, J. Am. Chem. Soc. **137**, 10148 (2015).

[60] A. Casaca, E. B. Lopes, A. P. Gonçalves, and M. Almeida, Electrical transport properties of CuS single crystals, J. Phys.: Condens. Matter **24**, 015701 (2012).

[61] A. L. Chen, S. P. Lewis, Z. Su, P. Y. Yu, and M. L. Cohen, Superconductivity in arsenic at high pressures, Phys. Rev. B **46**, 5523 (1992).

[62] K. Aoki, O. Shimomura, and S. Minomura, Crystal structure of the high-pressure phase of tellurium, J. Phys. Soc. Jpn. **48**, 551 (1980).

[63] C. Hejny and M. I. McMahon, Complex crystal structures of Te-II and Se-III at high pressure, Phys. Rev. B **70**, 184109 (2004).

[64] Y. Akahama, M. Kobayashi, and H. Kawamura, Structural studies of pressure-induced phase transitions in selenium up to 150 GPa, Phys. Rev. B **47**, 20 (1993).

[65] L. Zhao, C. Pei, J. Wu, Y. Zhao, Q. Wang, B. Zhu, C. Li, W. Cao, and Y. Qi, Superconductivity and critical fields of tellurium single crystal under high pressure, Phys. Rev. B **108**, 214518 (2023).

[66] H. Miao, G. Fabbris, R. J. Koch, D. G. Mazzone, C. S. Nelson, R. Acevedo-Esteves, G. D. Gu, Y. Li, T. Yilimaz, K. Kaznatcheev, E. Vescovo, M. Oda, T. Kurosawa, N. Momono, T. Assefa, I. K. Robinson, E. S. Bozin, J. M. Tranquada, P. D. Johnson, and M. P. M. Dean, Charge density waves in cuprate superconductors beyond the critical doping, npj Quantum Mater. **6**, 31 (2021).

[67] K. Machida, Spin density wave and superconductivity in highly anisotropic materials, J. Phys. Soc. Jpn. **50**, 2195 (1981).

[68] A. Ptok, M. M. Maśka, and M. Mierzejewski, Coexistence of superconductivity and incommensurate magnetic order, Phys. Rev. B **84**, 094526 (2011).

[69] D. F. Agterberg, J. C. S. Davis, S. D. Edkins, E. Fradkin, D. J. Van Harlingen, S. A. Kivelson, P. A. Lee, L. Radzihovsky, J. M. Tranquada, and Y. Wang, The physics of pair-density waves: Cuprate superconductors and beyond, Annu. Rev. Condens. Matter Phys. **11**, 231 (2020).